physica status solidi b
www.pss-b.com

High-Frequency Electron Paramagnetic Resonance and Electron-Nuclear Double Resonance Spectroscopy Study of the Ga Vacancy in β-Ga_2O_3

Hans Jurgen von Bardeleben and Jean Louis Cantin*

The Ga vacancy (V_{Ga}) defect in β-Ga_2O_3, generated by proton irradiation, is studied using high-frequency electron paramagnetic resonance (EPR) and electron-nuclear double resonance spectroscopy. The previous X-band EPR studies of this defect, attributed to V_{Ga}^{2-}, are extended to higher frequencies (240 GHz) and lower temperatures ($T = 6$ K). The spin Hamiltonian parameters of the V_{Ga}^{2-} center are determined: electron spin $S = 1/2$, g-tensor: $g_b = 2.0313$, $g_c = 2.0079$, and $g_a = 2.0025$; the hyperfine interaction parameters with 2 equivalent Ga neighbors: $A_b = 14.0$ G, $A_c = 14.6$ G, and $A_{a^*} = 12.8$ G for ^{69}Ga; the superhyperfine interaction with distant Ga neighbors $A_{SHF}(^{69}Ga) = 11$ MHz; and the quadrupole interaction $Q_b(^{69}Ga) = 0.32$ MHz and $Q_b(^{71}Ga) = 0.22$ MHz. These results shall allow to refine the assignment of this center to a split vacancy or an unrelaxed V_{Ga}^{2-} defect.

1. Introduction

Vacancy defects in ultrawide bandgap semiconductors such as β-Ga_2O_3 play an important role in their electronic properties.[1–3] They can be present as native defects in nonstoichiometric crystal growth or generated by high-energy particle irradiation or by high-temperature annealing.[4–9] In monoclinic β-Ga_2O_3, both Ga and O vacancies have been the object of different theoretical[3] and experimental studies. In β-Ga_2O_3, a large variety of different monovacancy defects might occur as two distinct Ga lattice sites and three distinct O sites have to be considered. The two Ga atoms are labeled Ga_I and Ga_{II} for the fourfold and sixfold oxygen coordinated sites, and the three O atoms O_I,O_{II}, and O_{III} are either threefold or fourfold Ga coordinated. Thus, different Ga and O monovacancies are expected to be formed. In addition, for the Ga vacancy, more complex configurations have been proposed. In fact, the split vacancy V_{GaI}–Ga_i–V_{GaI} is believed to be the most stable configuration of the V_{GaI} vacancy in the 3-charge state.[3] Ga vacancies are triple acceptors with charge states 3-/2-/1-/0. In n-type material, they will be in the 3-charge state but in the 2-charge state in semi-insulating Fe-doped material. Ga vacancies are paramagnetic in the 2- and 1-charge states with electron spin $S = 1/2$ and $S = 1$ respectively and can then be studied by electron paramagnetic resonance (EPR) spectroscopy. Both V_{Ga}^{2-} and V_{Ga}^{-} have been studied by X-band EPR spectroscopy.[5] The V_{Ga} centers were not observed by EPR in as-grown bulk samples neither in n-type nor in semi-insulating material but only after particle irradiation or high-temperature annealing. However, the high-temperature generated V_{Ga}^{2-} center is different from the irradiation-induced one and characterized by a two times higher HF interaction.[8,9] The issue of the microscopic model of the V_{Ga} centers is not yet settled.

Ga vacancies have been also investigated by positron annihilation spectroscopy (PAS).[10–12] By this technique, negatively charged vacancies irrespective of their magnetic properties can be detected. By PAS, vacancy centers have been observed in as-grown EFG bulk materials and based on theory results related to Ga vacancy centers. Surprisingly high concentrations $>10^{18}$ cm^{-3} of native vacancies in bulk samples have been deduced.[10,11] Ga vacancy defects being triple acceptors should lead to heavily compensated samples. The presence of high concentrations of native V_{Ga} centers is not supported by our EPR investigations, which have not detected any V_{Ga}-related defect in as-grown semi-insulating Fe-doped or n-type Sn-doped bulk samples. As V_{Ga} centers are expected to be in the 3-charge state in n-type material and thus nondetectable by EPR, this might explain the absence of observation. However, in semi-insulating Fe-doped material, the V_{Ga} centers are in the paramagnetic 2-charge state and should have been observed by EPR.

PAS spectroscopy is not a technique allowing to deduce absolute defect concentrations directly. The determination of defect concentrations is based on the trapping coefficient, which has only been assumed to be similar to previous oxide materials. To resolve this issue, it would be of interest to correlate PAS and quantitative EPR measurements in order to experimentally determine the trapping coefficient in β-Ga_2O_3.

H. J. von Bardeleben, J. L. Cantin
CNRS
Institut des NanoSciences de Paris
INSP
UMR7588
Sorbonne Université
F-75005 Paris, France
E-mail: vonbarde@insp.jussieu.fr

The ORCID identification number(s) for the author(s) of this article can be found under https://doi.org/10.1002/pssb.202400486.

DOI: 10.1002/pssb.202400486

Further, from PAS experiments, the native V_{Ga} defects have been attributed to split interstitial configurations, and very recently, the proton irradiation induced V_{Ga} to unrelaxed vacancies.[11] These models are at odds with the previous conclusions of the EPR results, which favored the split interstitial configuration for irradiation-induced V_{Ga}.[5] The microscopic structure of the native and irradiation-induced V_{Ga} centers clearly requires further experimental investigations and electron-nuclear double resonance spectroscopy (ENDOR) measurements can be expected to clarify this issue.

The V_{Ga}^{2-} centers are characterized by their spin Hamiltonian parameters: principal values and axes orientation of the g-tensor and their hyperfine (HF) interaction with the neighbor Ga atoms. In the previous studies on neutron, electron, and proton irradiated samples, similar but slightly different principal values of the g-tensor have been reported.[4–6] The principal axes of the g-tensor are parallel to the *b*-axis and in the a–c plane close to the *a*- and *c*-axes. A further characteristic of the V_{Ga}^{2-} center is the hyperfine interaction with two equivalent Ga neighbor atoms. None of the models considered was fully coherent with the experimental EPR results.[5] To refine the models of the native and process-induced V_{Ga} centers, first principle calculations of the g-tensor and hyperfine parameters as well as additional parameters such as quadrupole interactions and optical properties are required. In this work, we focused on the proton irradiation-induced V_{Ga}^{2-} center. In order to get more information on its microscopic structure, we have performed EPR measurements at higher frequencies and lower temperature ($T = 6$ K) and completed them with high-frequency ENDOR measurements.

2. Results and Discussion

In **Figure 1**a, we show a large-scale 240 GHz EPR spectrum for $B//b$. We observe, in addition to the V_{Ga}^{2-} spectrum, different EPR spectra, which from their spin Hamiltonian parameters can be attributed to Fe^{3+} (Ga_I), Fe^{3+} (Ga_{II}), and Cr^{3+} (Ga_{II}). Fe^{3+} centers are spin $S = 5/2$ centers with lattice site-dependent zero-field splitting parameters; the Cr^{3+} is a spin $S = 3/2$ center occupying the Ga_{II} lattice site preferentially. At 240 GHz, the resonance fields of the different centers are around $B = 8$ T.

Table 1. EPR parameters deduced from the 240 GHz EPR measurements at $T = 10$ K.

	g-values	SH parameters [10^{-4} cm^{-1}]	Literature values
Cr^{3+}(GaII)	$g_a = 1.96$	$b_{20} = 4752$	$b_{20} = 4753$
	$g_b = 1.96$	$b_{22} = 4701$	$b_{22} = 4227$[14]
	g_c[a)] $= 1.97$	$b_{21} = 8655$	$b_{21} = 8655$
Fe^{3+}(GaI)	$g = 2.002$	$b_{20} = -1427$	$b_{20} = -1570$
		$b_{22} = 1741$	$b_{22} = 1350$[13]
Fe^{3+}(GaII)	$g = 2.002$	$b_{20} = -2480$	$b_{20} = -2213$
		$b_{22} = 2293$	$b_{22} = 2091$[13]

[a)]The orientation 90° from the *a*-axis as the crystal *c*-axis is 103° from *a*.

Thus, the Zeeman levels of the Fe^{3+} and Cr^{3+} centers are only partially occupied at low temperature, and thus, only the lowest EPR transitions $\Delta ms = 1$ are observed (Figure 1b). The depopulation of the levels allows a direct determination of the sign of the zero-field splitting parameter b_{20}. The spin Hamiltonian parameters of the three defects given in **Table 1** are close to the previously published values with the exception of the value of Fe^{3+}, which can be determined with higher precision at this frequency.[13,14]

In **Figure 2**a, we show the EPR spectra of the V_{Ga}^{2-} center for the orientation of the magnetic field $B//b$ axis at 240 GHz and $T = 6$ K and compare it in Figure 2b to the one obtained at 9 GHz and $T = 60$ K; the spectrum simulations carried out with the EasySpin software are also shown.

Remarkably, the EPR linewidth is only slightly increased from $\Delta B = 4$–6 G, and thus, the HF structure is well resolved at 240 GHz. The HF splitting is identical to the one measured at 9 GHz and $T = 60$ K, and thus, dynamical effects to explain the equivalence of the two Ga neighbors can be excluded. At X-band frequency, the EPR spectrum of V_{Ga}^{2-} saturates strongly below $T < 40$ K and cannot be observed at $T = 6$ K. Attempts for ENDOR measurements at X-band frequency were unsuccessful.

In **Figure 3**a, we show the 240 GHz ENDOR spectrum with the magnetic field set at the central EPR line. As the RF frequency is not modulated, the ENDOR spectrum has an

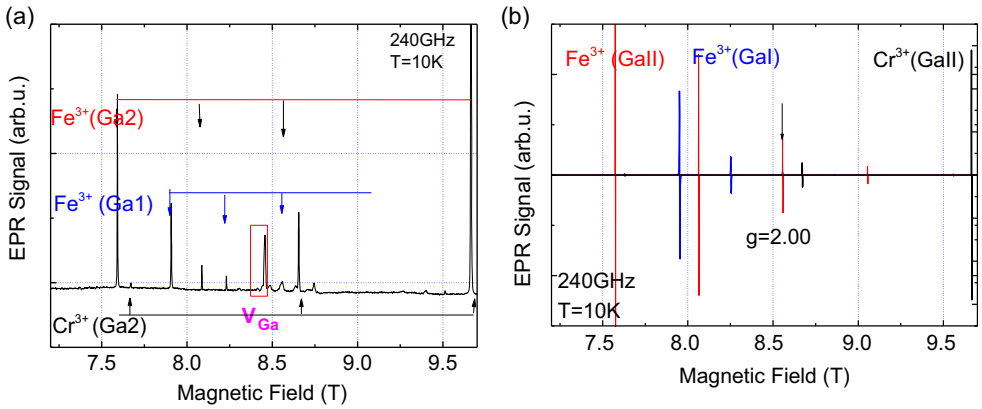

Figure 1. a) Large scale EPR spectrum at $T = 10$ K showing the native transition metal impurities Fe^{3+} on the Ga_I and Ga_{II} lattice sites and Cr^{3+} on the Ga_{II} lattice site and b) simulation of the Fe^{3+}, Cr^{3+} spectra for $B//b$ at $T = 10$ K.

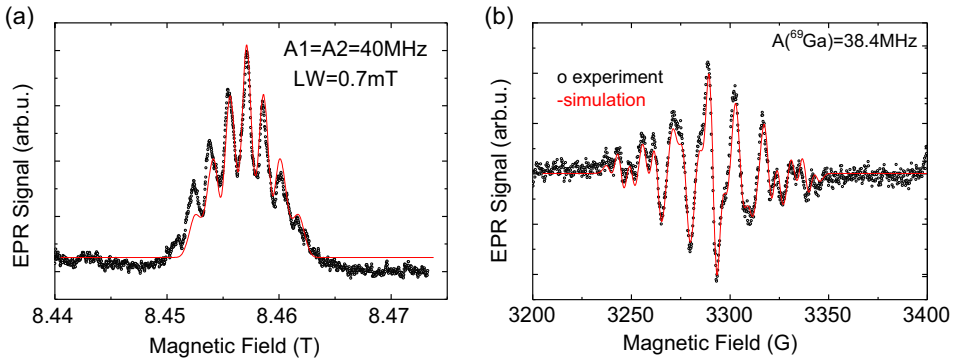

Figure 2. a) 240 GHz EPR spectrum of the V_{Ga}^{2-} center for $B//b$ at $T = 6$ K; black dots experiment, red line simulation and b) 9 GHz EPR spectrum for $B//b$ at $T = 60$ K; black dots experiment, red line simulation.

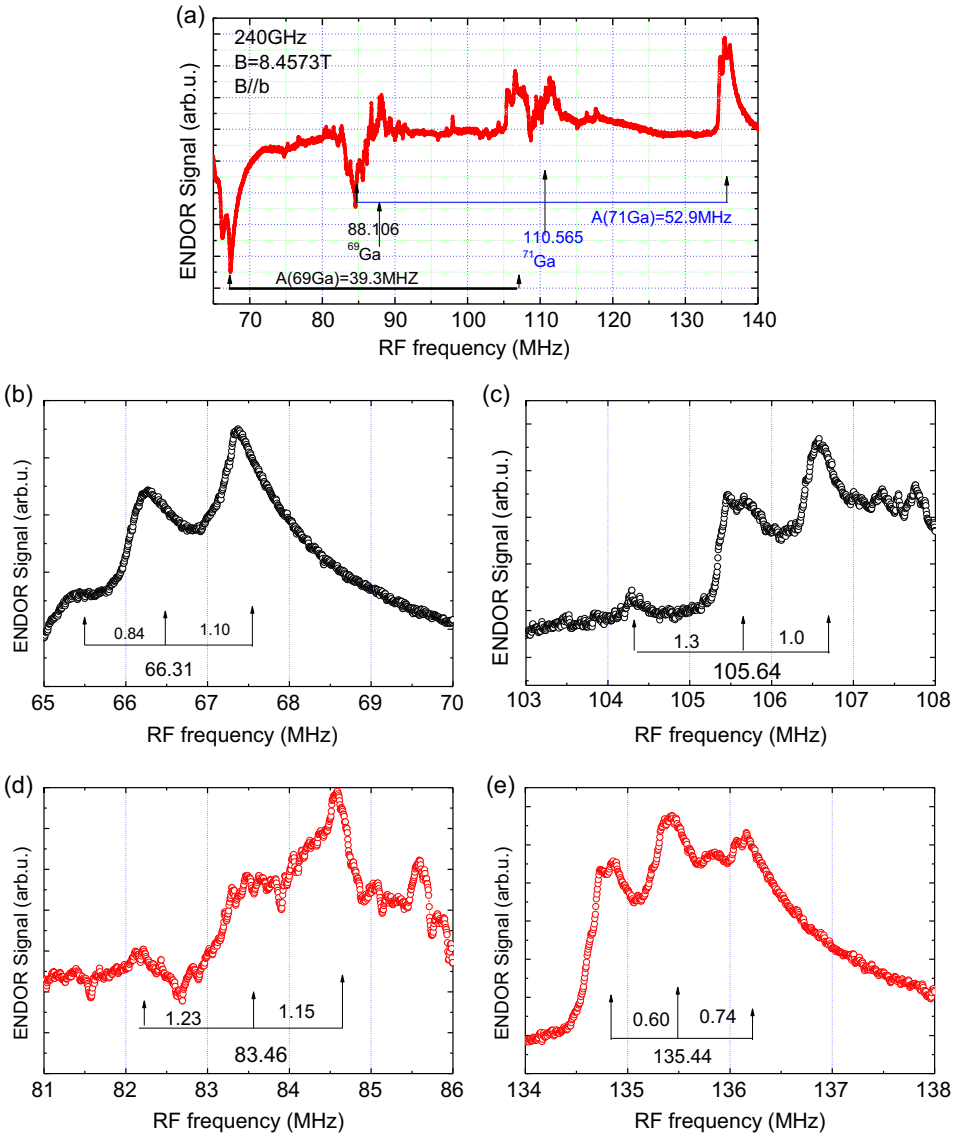

Figure 3. a) 240 GHz ENDOR spectrum of the V_{Ga}^{2-} center for $B//b$ at $T = 6$ K; $B = 8.4573$ T. b,c) Quadrupole splitting of the ENDOR lines of ^{69}Ga. d,e) Quadrupole splitting of the ENDOR lines of ^{71}Ga.

absorption shape and not a typical first derivative line shape. We observe ENDOR transitions between 65 and 140 MHz. At 240 GHz, the central EPR transition is at 8.4573 T, and thus, the nuclear Zeeman transitions for the ^{69}Ga and ^{71}Ga nuclei are situated at 88.1 MHz for the ^{69}Ga and 110.6 MHz for the ^{71}Ga atom. The spin Hamiltonian of this system is

$$H = \beta SgB + \sum_{i=1}^{2} (SA_iI_i + I_iQ_iI_i - g_{(n,i)}\beta_n I_i B) \quad (1)$$

In a first-order approximation, we can analyze the ENDOR spectrum considering each nucleus independent. When the intensities of nuclear Zeeman, hyperfine, and quadrupole interactions are respectively in the order: $\nu_N > \nu_{HF} > \nu_Q$, we expect to observe the HF transitions symmetrically around the nuclear Zeeman (ν_N) frequency, at $\nu_N + A/2$ and $\nu_N - A/2$. They are further split by the quadrupole interaction in three lines, corresponding to the nuclear transitions $m_I = 3/2 \text{-->} m_I = 1/2$, $m_I = 1/2 \text{-->} m_I = -1/2$, $m_I = -1/2 \text{-->} m_I = -3/2$. The analysis of the ENDOR spectrum is complicated by the fact that in the central part, the nuclear Zeeman transitions overlap with the HF lines. We obtain for this orientation $B//b$ HF interactions of $A(^{69}\text{Ga}) = 39.3$ GHz and $A(^{71}\text{G}) = 51.9$ MHz. The analysis of the central part around the nuclear Zeeman transitions indicates further superhyperfine interactions of $A(^{69}\text{Ga}) = 11$ MHz with distant Ga neighbors, but their detailed analysis requires additional experiments.

The quadrupole splitting of the ENDOR transitions for both ms = 1/2 manifolds are well resolved (**Table 2**), and we deduce values of $\nu_Q = 0.84$ MHz, $\nu_Q = 1.10$ MHz for the low-frequency ENDOR line of ^{69}Ga (Figure 3b), and $\nu_Q = 0.60$ MHz, $\nu_Q = 0.74$ MHz for the high-frequency ENDOR line of ^{71}Ga (Figure 3e), which we can compare to the respective electric quadrupole moments of ^{69}Ga and ^{71}Ga respectively: $m_Q(^{69}\text{Ga}) = 0.168 \times 10^{-24}\,\text{cm}^2$ and $m_Q(^{71}\text{Ga}) = 0.106 \times 10^{-24}\,\text{cm}^2$. Due to the relative signs of the hyperfine and quadrupole interactions, the splittings are different for the two ms = 1/2 states as shown in Figure 3b–e. Whereas the quadrupole splitting of each ENDOR line should give rise to triplets with an intensity ratio of 1:2:1, this is not always observed here, which we ascribe to the effect of dynamic nuclear polarization effects.

Table 2. EPR parameters of the irradiation-induced V_{Ga}^{2-} center.

		g-values	SH parameters A(^{69}Ga) (G)), Q [MHz]	References
V_{Ga}^{2-} EPR 9 GHz	Proton irradiated	g_a[a)] = 2.0025 g_b = 2.0313 g_c = 2.0079	A_a[a)] = 12.8 A_b = 13.8 A_c = 14.6	[4,5]
EPR 240 GHz ENDOR 240 GHz	Proton irradiated	–	A_b = 14.3 A_b = 14.0 6Qzz(^{69}Ga) = 1.94 MHz 6Qzz(^{71}Ga) = 1.34 MHz	This work
V_{Ga}^{2-} EPR 9 GHz	Neutron irradiated	g_a = 2.0034 g_b = 2.0322 g_c = 2.0097	A_{a*} = 12.8 A_b = 14.4 A_c = 13.6	[6]

[a)]The orientation 90° from the *a*-axis as the crystal *c*-axis is 103° from *a*.

To relate the observed quadrupole splittings to the Ga_I or Ga_{II} lattice sites, first principle calculations are required. The results should allow to compare the models of the split interstitial V_{GaI}–Ga_i–V_{GaI} and the simple mono vacancy models suggested by PAS spectroscopy and locate the spin density on the O_I, O_{II}, or O_{III} sites. Such calculations are now underway.

3. Conclusion

In conclusion, we have investigated the EPR and ENDOR spectra of the irradiation-induced V_{Ga}^{2-} center at 240 GHz and low temperature of $T = 6$ K for the canonical orientation $B//b$. Our results exclude motional effects to explain the equivalence of the two Ga neighbors. The quadrupole interaction parameter has been determined and its value will be a main parameter for the modeling of the microscopic structure of the defect.

4. Experimental Section

β-Ga_2O_3(010) oriented unintentionally doped (UID) bulk samples of 400 μm thickness were purchased from Tamura Corp; they were grown by edge-defined film-fed technique (EFG); n-type conducting, nonintentionally doped, and semi-insulating Fe-doped bulk samples have been investigated. Typical carrier concentrations in the UID-doped samples were $(N_D - N_A) = 2 \times 10^{17}\,\text{cm}^{-3}$. They were irradiated at room temperature with 12 MV protons with a fluence of $1 \times 10^{15}\,\text{cm}^{-2}$. After this irradiation, the n-type samples were semi-insulating and showed no longer a shallow donor resonance. The size of samples was $2 \times 3\,\text{mm}^2$ with a rectangular shape with axes along and perpendicular to [102]. The high-frequency EPR measurements were performed at 240 GHz and at temperatures in the range $T = 6$–10 K. The high-frequency ENDOR measurements were obtained with low-frequency magnetic field modulation of the EPR spectrum and sweeps of nonmodulated RF radiation in the range 60–150 MHz. The EPR/ENDOR measurements were performed for three orientations of the applied magnetic field $B//b$ axis and two orientations in the *a*–*c* plane. In this work, we will mainly discuss the results for $B//b$.

Acknowledgements

The authors thank H. van Tol at the NHFL in Tallahassee (Florida) for the high-frequency measurements and V. Soltamov (Kazan University) and L. Binet (Sorbonne University) for helpful discussions. H.J.v.B. and J.L.C. acknowledge financial support from the French National Agency (ANR), project "GOPOWER," grant no. (CE-50 N0015-01).

Conflict of Interest

The authors declare no conflict of interest.

Data Availability Statement

The data that support the findings of this study are available from the corresponding author upon reasonable request.

Keywords

electron-nuclear double resonance spectroscopy, gallium oxides, gallium vacancies, proton irradiations

Received: September 13, 2024
Revised: October 23, 2024
Published online:

[1] M. D. McCluskey, *J. Appl. Phys.* **2020**, *127*, 101101.
[2] C. Zimmermann, V. Ronning, Y. K. Frodason, V. Bobal, L. Vines, *Phys. Rev. Mater.* **2020**, *4*, 074605.
[3] J. M. Johson, Z. Chen, J. B. Varley, C. M. Jackson, E. Farzana, Z. Zhang, A. R. Arehart, H. L. Huang, A. Genc, S. A. Ringel, C. G. Van de Walle, *Phys. Rev. X* **2019**, *9*, 041027.
[4] H. J. von Bardeleben, S. Zhou, U. Gerstmann, D. Skachkov, W. L. Lambrecht, Q. D. Ho, P. Deak, *APL Mater.* **2019**, *7*, 022521.
[5] D. Skachkov, W. L. Lambrecht, H. J. von Bardeleben, U. Gerstmann, Q. D. Ho, P. Deak, *J. Appl. Phys.* **2019**, *125*, 185701.
[6] B. E. Kananen, L. E. Halliburton, K. T. Stevens, G. K. Foundos, N. C. Giles, *Apl. Phys. Lett.* **2017**, *110*, 202104.
[7] J. McGlone, H. Ghadi, E. Cornuelle, A. Armstrong, G. Burns, Z. Feng, A. F. M. Anhar Uddin Bhuiyan, H. Zhao, A. R. Arehart, S. A. Ringel, *J. Appl. Phys.* **2023**, *133*, 045702.
[8] N. T. Son, Q. D. Ho, K. Goto, H. Abe, T. Ohshima, B. Monemar, Y. Kumagai, T. Frauenheim, P. Deák, *Appl. Phys. Lett.* **2020**, *117*, 032101.
[9] H. J. von Bardeleben, G. He, Y. Wu, S. Ding, *J. Appl. Phys.* **2023**, *134*, 165702.
[10] A. Karjalainen, I. Makkonen, J. Etula, K. Goto, H. Murakami, Y. Kumagai, F. Tuomisto, *Appl. Phys. Lett.* **2021**, *118*, 072104.
[11] I. Zhelezova, I. Makkonen, F. Tuomisto, *J. Appl. Phys.* **2024**, *136*, 065702.
[12] F. Tuomisto, *Jpn. J. Appl. Phys.* **2023**, *62*, SF0802.
[13] M. L. Meilman, I. A. Gavrilov, *Sov. Phys. Solid State* **1969**, *11*, 628.
[14] J. E. Stehr, M. Jansson, D. M. Hofmann, J. Kim, S. J. Pearton, W. M. Chen, I. A. Buyanova, *Appl. Phys. Lett.* **2021**, *119*, 052101.